Journal of Hydrology (2008) 361, 41–51

available at www.sciencedirect.com

ScienceDirect

journal homepage: www.elsevier.com/locate/jhydrol

Relating small-scale sedimentary structures and permeability in a cross-bedded aquifer

Marijke Huysmans [a,*], Luk Peeters [a], Gert Moermans [a], Alain Dassargues [a,b]

[a] *Katholieke Universiteit Leuven, Applied Geology and Mineralogy, Department of Earth and Environmental Sciences, Celestijnenlaan 200 E, 3001 Heverlee, Belgium*
[b] *Université de Liège, Hydrogeology and Environmental Geology, Department of Architecture, Geology, Environment, and Civil Engineering (ArGEnCo), B.52/3 Sart-Tilman, 4000 Liège, Belgium*

Received 25 January 2008; received in revised form 25 June 2008; accepted 11 July 2008

KEYWORDS
Geological heterogeneity;
Sedimentary structures;
Air permeability;
Geostatistics;
Belgium

Summary The objective of this study is to investigate the relation between small-scale sedimentary structures and permeability in the Brussels Sands formation, an early Middle-Eocene shallow marine sand deposit in Central Belgium that constitutes a major groundwater source in the region. A field campaign was carried out consisting of field observations of the sedimentary structures and in situ measurements of air permeability. The sedimentary structures were interpreted, sketched, digitally photographed and measured in a representative outcrop. Additionally, a total of 2750 cm-scale air permeability measurements were carried out in situ. Analysis of the spatial distribution of sedimentary structures and permeability shows that clay-rich sedimentary features such as bottomsets and distinct mud drapes exhibit a different statistical and geostatistical permeability distribution compared to the other lithofacies in the cross-bedded sands. Spatial analysis of the air permeability data shows that permeability anisotropy in the cross-bedded lithofacies is dominated by the foreset lamination orientation. These results show that small-scale sedimentary heterogeneity strongly influences the local spatial distribution of the hydraulic properties and results in permeability heterogeneity and stratification that would produce anisotropy in upscaled permeability values.

Introduction

Sedimentological and erosional processes often result in a complex three-dimensional subsurface architecture of sedimentary structures and facies types. Such complex sedimentological heterogeneity may induce a highly heterogeneous spatial distribution of hydrogeological parameters

* Corresponding author. Tel.: +32 16 32 64 49; fax: +32 16 32 29 80.
E-mail address: marijke.huysmans@geo.kuleuven.be (M. Huysmans).

0022-1694/$ - see front matter © 2008 Elsevier B.V. All rights reserved.
doi:10.1016/j.jhydrol.2008.07.047

in porous media at different scales (Davis et al.,1993, 1997; Klingbeil et al., 1999; Ritzi et al., 2004) and may consequently greatly influence subsurface fluid flow and solute migration (Koltermann and Gorelick, 1996; Zheng and Gorelick, 2003; Zinn et al., 2004). Several previous papers discuss the role of sedimentological heterogeneity in hydrogeological case studies (e.g. Anderson, 1989; Fogg et al., 1998; Klingbeil et al., 1999; Heinz et al., 2003; Van den Berg and de Vries, 2003; Tipping et al., 2006). Most of these authors study sedimentological heterogeneity at relatively large scales treating each sedimentological facies as a homogeneous, anisotropic hydrogeologic unit. They usually do not address the small-scale heterogeneity present within individual facies. Small-scale or micro-scale permeability heterogeneity (≈1 mm to 10 m scale) related to small-scale sedimentary structures is usually not taken into account in groundwater and solute transport modeling. In petroleum reservoir modeling however, several authors acknowledge that cm-scale sedimentary heterogeneity plays an important role in oil recovery and that incorporating this small-scale sedimentary heterogeneity is required for reliable prediction of oil production (e.g., Mikes, 2006; Morton et al., 2002; Willis and White, 2000). Since this small-scale sedimentary heterogeneity plays such a significant role in reservoir modeling, it is likely that this may also be important in hydrogeological studies. Although petroleum production as a multiphase flow process could be more sensitive to local scale heterogeneity than groundwater flow and transport, the major role of small-scale sedimentary heterogeneity in reservoir modeling suggest that heterogeneity at this scale may also be important in hydrogeological studies, particularly in solute transport modeling. Therefore, this research project aims to examine and model the effect of cm-scale sedimentary heterogeneity on permeability heterogeneity and anisotropy and consequently on groundwater flow and contaminant transport in heterogeneous environments with complex geological structures. This paper focuses on the first part of this research project, which is an extensive field campaign to examine the relation between sedimentary structures and permeability in an aquifer exhibiting complex small-scale sedimentary heterogeneity.

Materials and methods

Geological setting

The aquifer under study is the Brussels Sands formation, which is a major source of groundwater in Belgium. Approximately 29,000,000 m^3 of groundwater per year is pumped from this aquifer. The Brussels Sands display a complex geological heterogeneity and anisotropy that complicates pumping test interpretation, groundwater modeling and prediction of pollutant transport.

The Brussels Sands formation is an early Middle-Eocene shallow marine sand deposit in Central Belgium (Fig. 1). The sands consist of unconsolidated quartz sands with variable percentages of feldspars, silex, glauconite, carbonates and heavy minerals. The Brussels Sands are a tidal sandbar deposit, deposited at the beginning of an important transgression at the southern border of the Eocene North Sea. The Brussels Sands base has an erosive character which is thought to be related to a strong SSW-NNE tidal current that produced longitudinal troughs. Transverse sandbars that migrated to the north filled these rapidly shifting channels. The tidal regime was strongly asymmetric and ebb-dominated with a NNE oriented main tidal flow. In a first depositional stage, large amounts of clastic sands mixed with

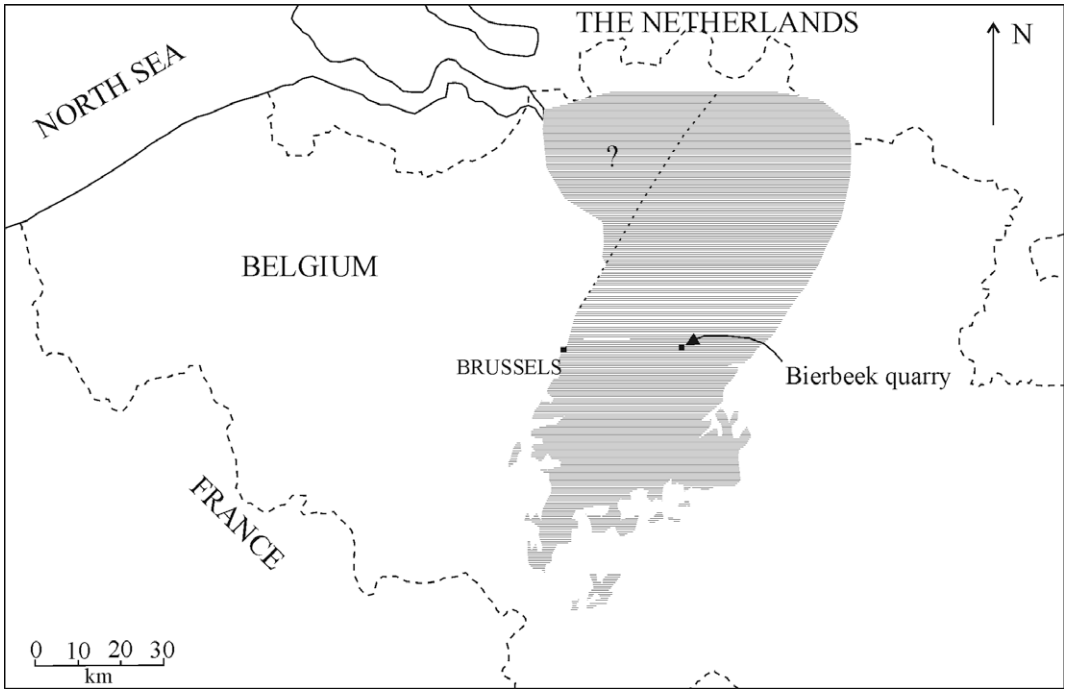

Figure 1 Map of Belgium showing Brussels Sands outcrop and subcrop area (shaded part) and the location of the Bierbeek quarry (modified after Houthuys (1990)).

coarse glauconite are deposited as thick cross-beds filling tide-parallel channels of a few kilometers wide and tens of meters deep. In a later depositional stage, the supply of glauconite ended and finer, carbonate-rich sands were deposited (Houthuys, 1990).

The depositional environment of the Brussels Sands is studied in detail by Houthuys (1990) based on field studies and descriptions of approximately 90 outcrops and hundreds of boreholes. His work describes several features and sedimentary structures typical for tidal deposits such as important grain size variations, cross-bedding, bottomsets, foresets, mud drapes and unidirectional reactivation surfaces (Fig. 2). Cross-bedding is defined as the disposition of laminations transverse or obliquely inclined to the main stratification of the bedding planes (Whittow, 2000). Cross-bedding in the Brussels Sands is caused by sediment deposition at the leeside of migrating sandbars. Bottomset beds are formed in front of the leeside of migrating sandbars and consist of finer grained sediment. Foreset deposits consist of laminae that formed by grains avalanching down the leeside of sandbars. The inclined foreset laminae are preserved in sequence in the sand bodies and are a record of successively earlier positions of the leesides. The grains are sorted during avalanching, resulting in coarse and fine grained laminae (Hartkamp et al., 1993). Mud drapes are thin layers of mud covering the complete seafloor during turning of the tide (Houthuys, 1990). Reactivation surfaces are produced when the lee side of a sandbar is partially eroded.

Field observations of sedimentary structures

Several authors report successes in hydrogeological parameter estimation from meso-scale (≈10 m to 5 km scale) to mega-scale (≈5—50 km scale) based on outcrop-based sedimentological interpretation (e.g. Goggin et al., 1988a; Klingbeil et al., 1999; Heinz et al., 2003; Ritzi et al., 2003; Sturgeon et al., 2006). A similar approach of sedimentological outcrop mapping on a more local scale was used in this study to investigate smaller scale sedimentary and hydraulic heterogeneity. The sedimentary structures of the cross-bedded facies of the Brussels Sands were described and interpreted in the Brussels Sands quarry in Bierbeek near Leuven in Belgium (Fig. 1). A movie showing a panoramic view of the quarry can be found at: http://www.zandgroeven-bouillon.be/bedrijf/pano.html. This outcrop can be assumed as representative for the sandbar facies of the Brussel Sands according to the work of Houthuys (1990). The outcrop of approximately 1200 m^2 was mapped in detail with regard to the spatial distribution of sedimentary structures and lithologies. Geological sketches and digital photographs from all faces of the quarry were made. Clay-rich bottomsets and distinct mud drapes in the foresets were visually identified on the surface outcrops based on sediment characteristics. Measurements were made of the set thicknesses, master bedding dipping angles, bottomset thicknesses, foreset lamination thicknesses and lamination dipping angles. These measurements were compared with data from Houthuys (1990) and analyzed statistically.

In situ permeability measurements

To investigate the relationship between sedimentary structures and permeability at a cm-scale to m-scale, pumping tests and slug tests are not useful since they provide permeability information on a much larger scale. Therefore, an in situ air permeameter was used to determine permeability at a small-scale. Air permeameters have been used in a wide variety of laboratory and field applications where localized small-scale measurements are needed to characterize the spatial distribution of permeability (e.g., Goggin et al., 1988a; Dreyer et al., 1990; Jacobsen and Rendall, 1991; Hartkamp et al., 1993; Tidwell and Wilson, 1999; Castle et al., 2004). Air permeameter measurements have the advantage to be cheap, rapid, nondestructive and readily

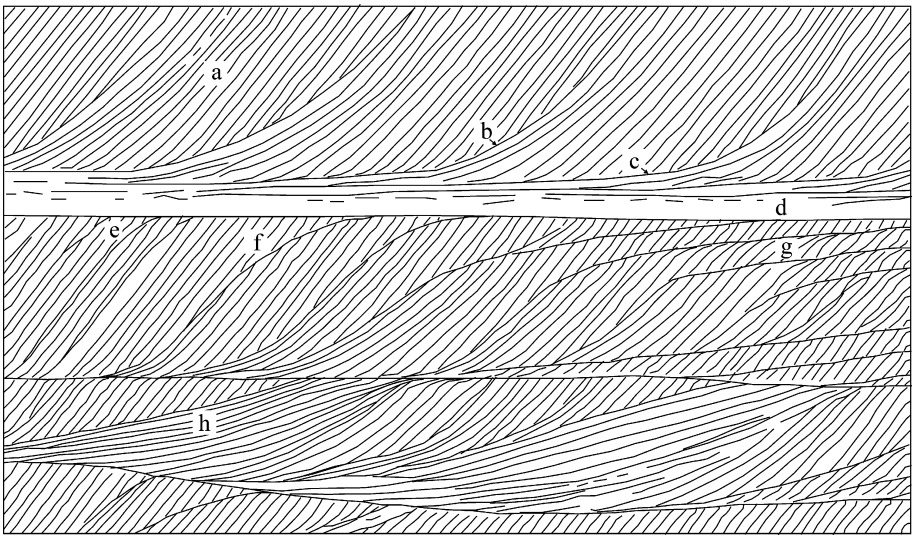

Figure 2 Sketch of sedimentary structures observed in Brussels Sands: (a) foreset laminae, (b) concave foreset laminae, (c) mud drapes, (d) bottomsets, (e) high-angle reactivation, (f) convex-upwards reactivation, (g) low-angle reactivations and (h) low-angle foreset lamination (modified after Houthuys (1990)). Height of sketch is approximately 3 m.

repeatable and can provide a high resolution, almost continuous profile of permeability distribution. In situ permeameters can reveal several orders of magnitude of permeability contrast missed by conventional core plug measurements (Goggin et al., 1988b; Halvorsen and Hurst, 1990). Air permeameter measurements are particularly suitable for poorly consolidated and laminated materials, both of which may present problems for permeability characterization using core plugs (Hurst and Goggin, 1995). Potential disadvantages of air permeability measurements are the sensitivity of probe permeameter response to partial or full saturation and sample surface effects such as irregularities and weathering, the limited knowledge about the geometry of flow paths in probe permeameter experiments and the requirement that outcrops should be completely dry or their relative permeability to gas and water should be known to allow satisfactory interpretation of the data.

A device for obtaining small-scale air permeability measurements was first described by Dykstra and Parsons (1950). Later, Eijpe and Weber (1971) constructed a minipermeameter for measuring the permeability of rock and unconsolidated sands. A probe permeameter is basically an annulus through which gas (nitrogen or air) can be released into porous media. Leakage between the annulus and the porous media is avoided by placing a ring of compressible, impermeable material at the probe tip. Gas flow rate and gas pressure are monitored and can be transformed into gas permeability by empirically derived relationships or by use of an analytical equation, such as the modified form of Darcy's law including a geometrical factor depending on tip seal size proposed by Goggin et al. (1988a, b):

$$k = 2\mu P_1 Q_1 / ((P_1^2 - P_2^2) G_0^a) \quad (1)$$

where k is permeability, μ is the gas viscosity at atmospheric pressure, P_1 is injection pressure, P_2 is outflow pressure, Q_1 is the volumetric rate at injection pressure P_1, G_0 is a dimensionless geometric factor and a is the radius of the seal area. For certain ranges of permeability, Eq. (1) should be corrected to account for gas slippage and high velocity gas flow effects (Goggin et al. 1988a, 1988b). The depth of investigation of a minipermeameter is approximately four times the internal radius of the tip seal according to Goggin et al. (1988a, 1988b). In an isotropic porous medium, the measurement volume corresponds to a hemispherical shaped volume of rock with radius of approximately four times the internal radius of the tip seal. Jensen et al. (1994) found that probe permeameter measurements are even more localized with a depth of investigation of the order of only two probe inner radii.

In this study, air permeability was measured using the TinyPerm II distributed by New England Research (NER). Permeability measurements were taken by pressing the device against the quarry face and depressing the plunger to

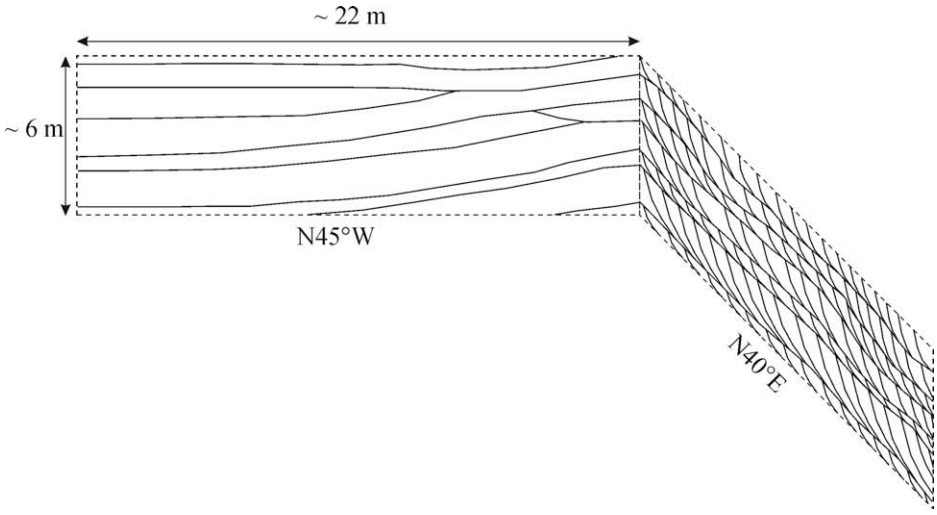

Figure 3 Sketch of bed geometry of Bierbeek quarry faces. Height of sketched walls is approximately 6 m.

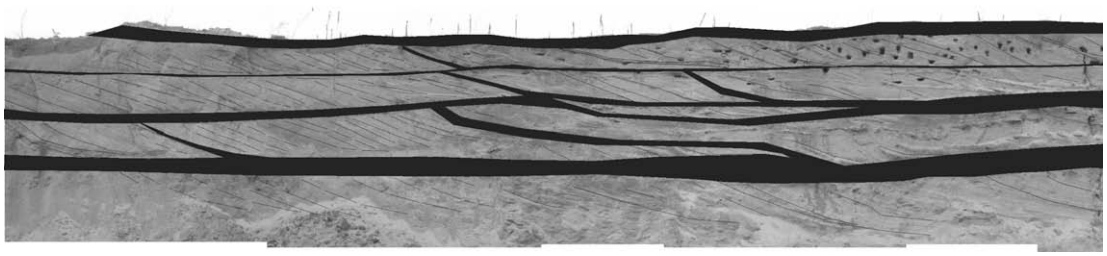

Figure 4 Interpreted photomosaic of quarry wall showing clay-rich bottomsets and distinct mud drapes in black. Height of quarry wall is approximately 4—5 m.

withdraw air from the porous medium. Leakage between the annulus and the rock is avoided by a compressible, impermeable rubber tip. The inner tip diameter is 9 mm and the outer tip diameter is 24 mm. According to the equations of Goggin et al. (1988a, 1988b), this means that the depth of investigation of TinyPerm is approximately 18 mm. The measurement volume is in this case a hemi-spherical shaped volume with a radius of approximately 18 mm. A micro-controller unit simultaneously monitors the syringe volume and the transient vacuum pulse created at the sample surface. Using signal processing algorithms the micro-controller computes the response function of the sample/instrument system. This response function is related to the air permeability of the sample, which can be

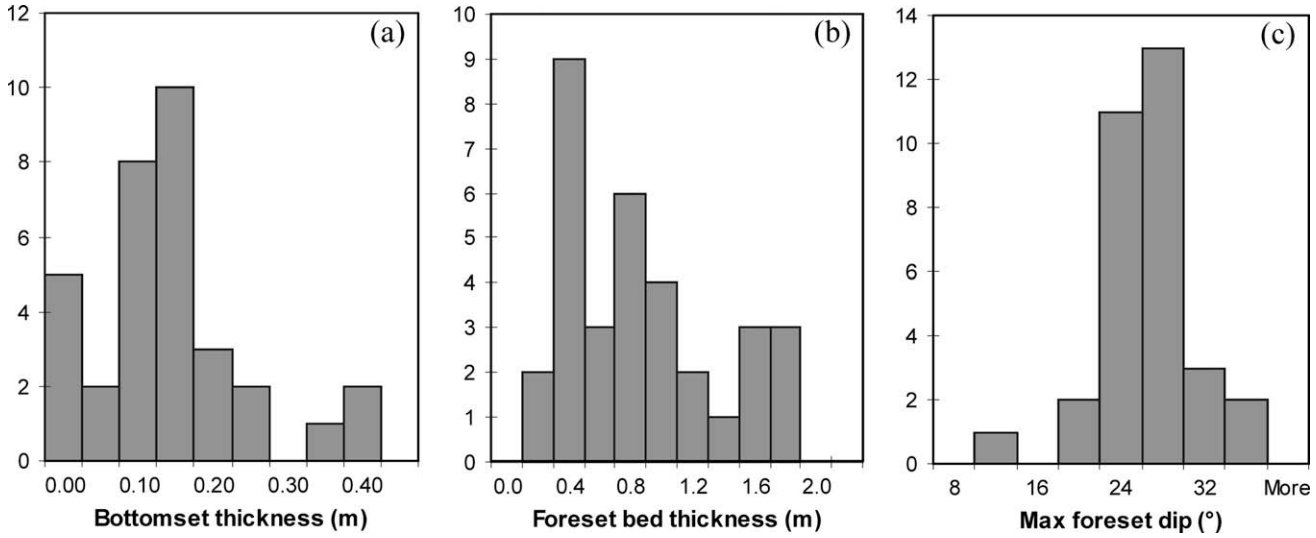

Figure 5 Histograms of (a) bottomset thicknesses, (b) set thicknesses and (c) lamination dipping angles.

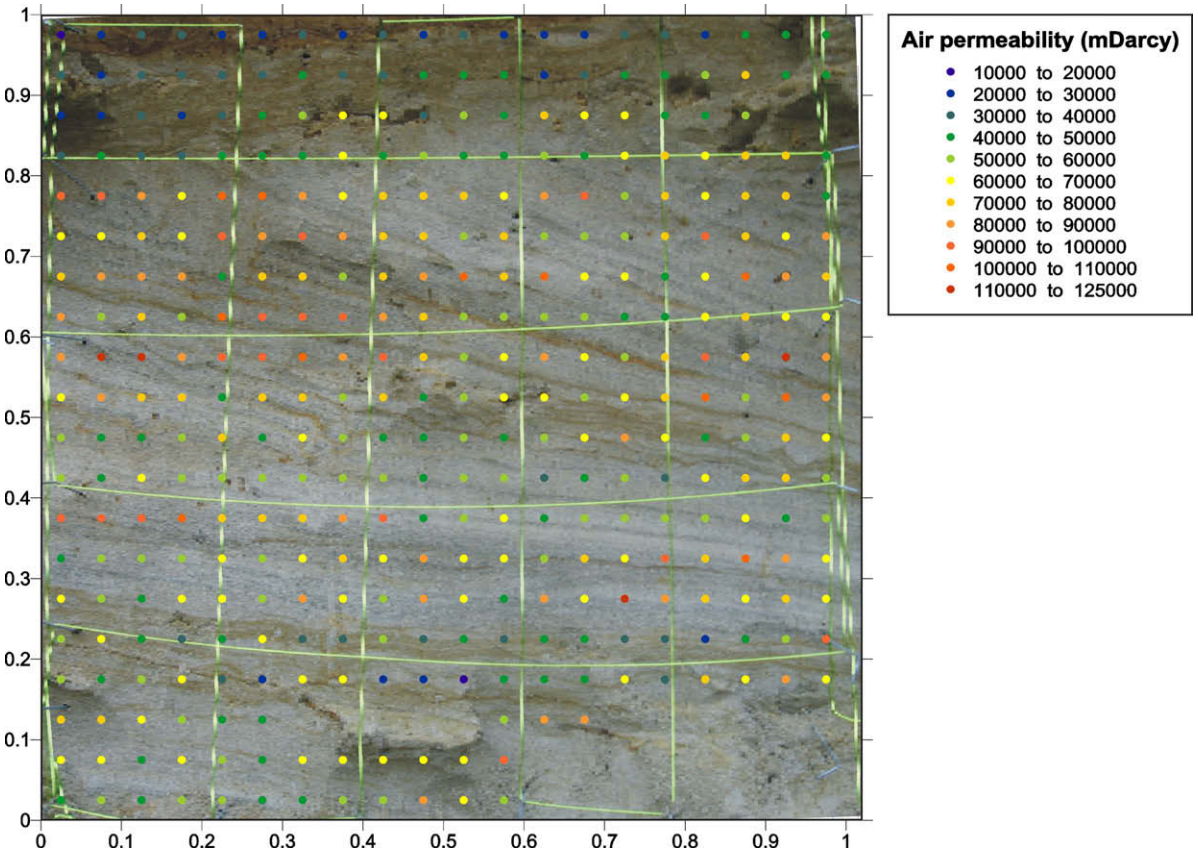

Figure 6 Air permeability (mD) projected on a field picture of a 1 m × 1 m 5 cm-spaced regular grid on a N40°E oriented face.

determined by an equipment specific calibration curve provided by NER. Measurements of high permeability samples take a few seconds, measurements of less permeable samples take up to a few minutes.

To prevent loose sand debris being sucked into the device, a metal screen was fitted in the rubber tip for this study. After installation of this filter, the TinyPerm II was recalibrated since the filter can impede air flow. Rock samples with different permeabilities were measured with and without the filter to obtain a calibration curve for the device equipped with a filter. The sample set for recalibration consists of seven sandstone samples, a limestone sample and a chalk sample. All rock samples have a smooth to slightly irregular surface. The permeabilities of the calibration set range from 1 to 10,000 milliDarcies (mD) which is within the measurement range of the TinyPerm II air permeameter. Each sample was measured six times: three times without filter and three times with filter. As expected, permeability values measured with the filter were slightly smaller than permeability values measured without the filter. Permeability values with filter were on average 89% of permeability values measured without filter. To correct for this effect, the TinyPerm II response function of the measurements with filter was plotted against the permeability values obtained without a filter using the calibration curve provided by NER. This yields a calibration curve for the device after installation of the filter.

Permeability of the Brussels Sands was measured on all faces of the Bierbeek quarry in Central Belgium using a portable in situ air permeameter. Measurements were taken on several rectangular regular grids on different walls in dry conditions. All irregularities and weathered or loose material was removed prior to constructing the grids. The measurement spacing was adjusted to the lamina thickness so that the vertical and horizontal spacing is between 2 cm and 5 cm. Total grid size is between 40 cm and 1 m. A total of approximately 2750 air permeability measurements were made on outcrops with different orientations in the Bierbeek quarry. The measured permeability values were compared with Brussels Sands permeability values from literature. The measured permeability values were also compared with the sedimentary facies and structures observed at the same location.

All 2750 permeability data were also analyzed statistically and geostatistically. Permeability variograms were calculated and modeled using Stanford Geostatistical Earth Modeling Software or S-GEMS (Remy, 2004). Previous papers consider the variogram as a very useful tool for interpreting and identifying geological structure in permeability fields (e.g., Jensen et al., 1996; McKinley et al., 2004). The variogram is the most familiar geostatistical estimator and is defined as half of the average squared difference between variable values separated by a lag vector **h** (Deutsch and Journel, 1998):

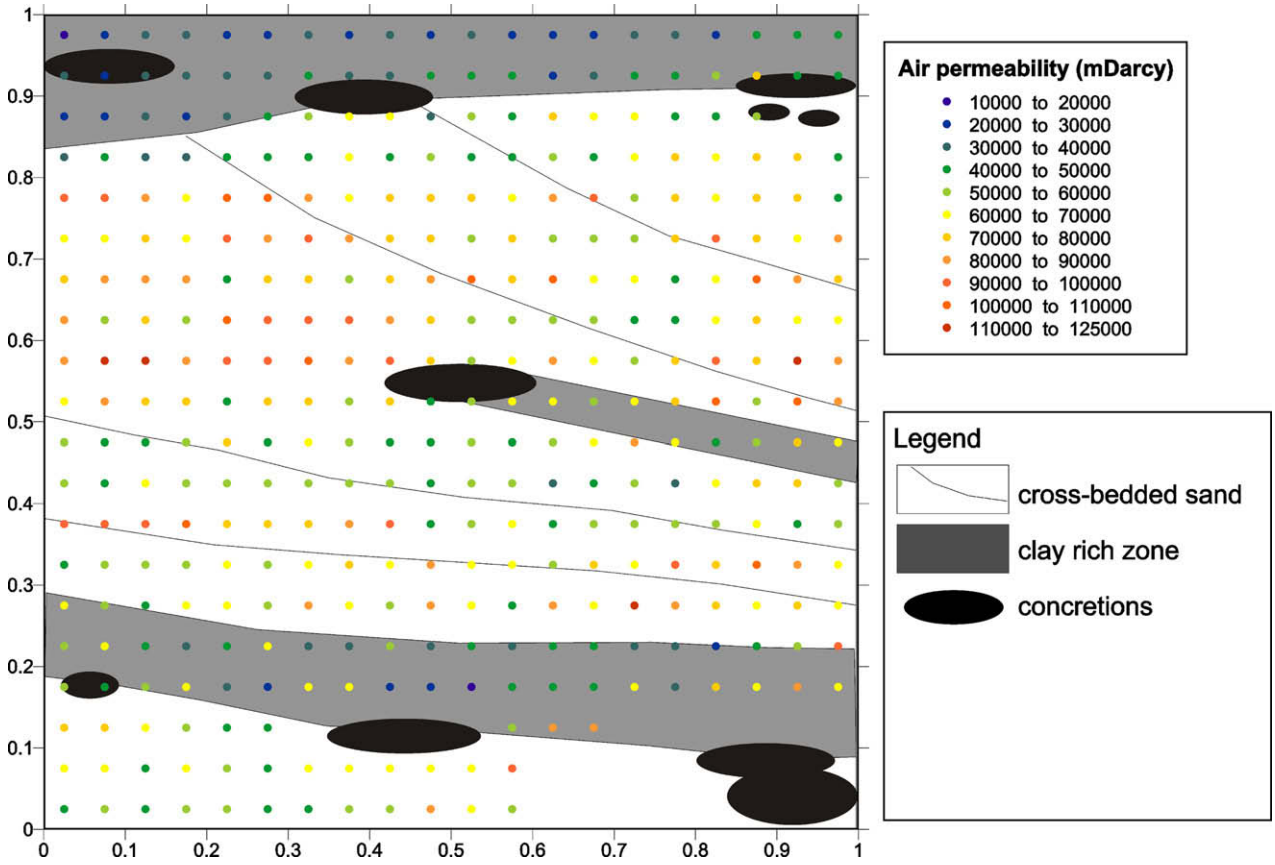

Figure 7 Air permeability (mD) projected on a geological sketch of a 1 m × 1 m 5 cm-spaced regular grid on a N40°E oriented face.

$$\gamma(\mathbf{h}) = 1/(2N(\mathbf{h}))\sum_{i=1}^{N(\mathbf{h})}(x_i - x_i')^2 \quad (2)$$

where $N(\mathbf{h})$ is the number of pairs and x_i and x_i' are a data pair separated by $\mathbf{h}$. The semivariogram can be understood as the sample variance described as a function of spatial separation. Low semivariogram values indicate a high degree of correlation between variable values separated by the lag vector, while high semivariogram values indicate a low degree of correlation. Spatial variability is often anisotropic so that variograms are different when taking into account different directions. In this case, variograms can be calculated in different orientations to construct a variogram map or a variogram surface that displays spatial variability in all directions. Variogram maps were calculated using Variowin (Pannatier, 1996).

Variograms are usually modeled with a variogram model. The model used in this study is the sum of a nugget model and a spherical model:

$$\gamma(\mathbf{h}) = \begin{cases} 0 & \text{if } h = 0 \\ C_0 + C(1.5(h/a) - 0.5(h/a)^3) & \text{otherwise} \\ C_0 + C & \text{if } h > a \end{cases} \quad (3)$$

where C_0 is the nugget effect, C is the sill and a is the range.

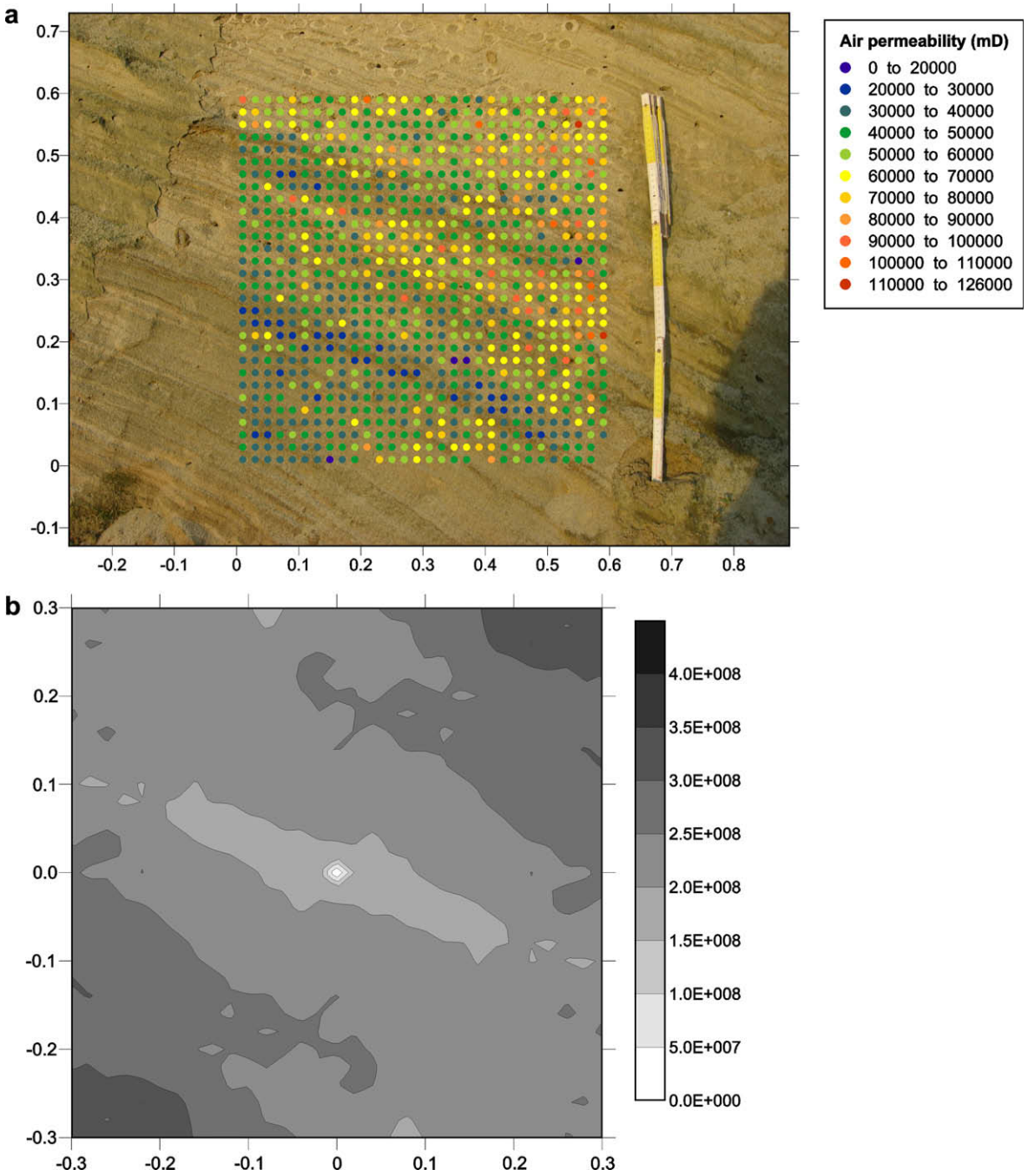

Figure 8 (a) Air permeability (mD) projected on a field picture of a 0.6 m × 0.6 m 2 cm-spaced regular grid on a N40°E oriented face and (b) variogram map of the same data.

Table 1 Permeability characteristics of the cross-bedded sands and clay-rich zones

	Sand facies	Clay-rich facies
Mean k (mD)	58,700	42,200
Variance k (mD)^2	3.6e8	2.55e8
Variogram type k	Spherical	Spherical
Nugget (mD)^2	2.09e8	1.03e8
Sill (mD)^2	1.51e8	1.52e8
Dip angle of major axis of anisotropy	26°	0° (horizontal)
Lamina parallel range (m)	0.6	1.9
Lamina perpendicular range (m)	0.3	0.4

Results and discussion

Sedimentary structures

The sedimentary structures observed in the Bierbeek quarry correspond to the descriptions of Houthuys (1990). The Brussels Sands in this quarry consist of parallel sub-horizontal tabular sets dipping approximately 1° to the NNE (Fig. 3). The set thickness is usually approximately 1 m and may be up to 2.5 m. Individual sets can be followed over distances as large as the quarry dimensions in the paleoflow direction. In a perpendicular section, individual sets dipping up to 5° occur in wedge-shaped groups alternately deposited on the east and west side of a channel. These individual sets can be followed over tens of meters in a section perpendicular to the paleoflow direction (Fig. 3). Most beds include a thick bottomset consisting of finer grained material at the base. These bottomsets are usually about 10 cm thick, and can be as thick as 50 cm. The bottomsets sometimes show a lateral thickness variation. The foresets have a lamination thickness of 0.5 to 3 cm and dip approximately 25—30° to the NNE. Thin mud drapes consisting of fine silt and clay occur in the foreset laminae resulting in grain size contrasts. The mud drapes are best developed near the toesets and wedge out in the upper part of the foresets. Lateral variations in the amount of mud drapes occur due to neap/spring cycles. Mud drapes are not always laterally continuous perpendicular to the paleoflow direction.

A visual distinction between sand-rich and clay-rich zones was made in situ based on sediment characteristics. The sand-rich zones consist of cross-bedded sand facies while the clay-rich zones consist of clay-rich bottomsets and distinct mud drapes inside the cross-beds. Twenty-three percent of the outcrop is classified as clay-rich zone while 77% of the outcrop is classified as cross-bedded sand facies. It should be noted that the clay-rich zones do not consist of pure clay. Grain size measurements from Houthuys (1990) indicate that the clay-rich zones consist of 20% of silt and clay. Fig. 4 shows an interpreted photomosaic of one of the quarry walls, corrected for perspective distortion. On this photograph, the clay-rich bottomsets and distinct mud drapes in the foresets that are visually identified in situ are marked.

Thickness and dip measurements of several sedimentary features were made at various locations in the quarry and analyzed statistically. Histograms of bottomset thicknesses, set thicknesses and lamination dipping angles measured during this measurement campaign combined with the data from Houthuys (1990) are shown in Fig. 5. Bottomset thickness varies between 0 and 38 cm in the Bierbeek area and is 11 cm on average. The average set thickness is 79 cm. Foreset lamination dip is between 10° and 33° with an average value of 25°.

Permeability

Measured air permeability using the TinyPerm air permeameter in the Bierbeek quarry lies between 11,000 mD and 125,000 mD. These values were compared to values derived from well tests carried out at different locations in the Brussels Sands. Hydraulic conductivity from pumping tests and piezometer tests is between 4.6×10^{-6} and 3.4×10^{-4} m/s

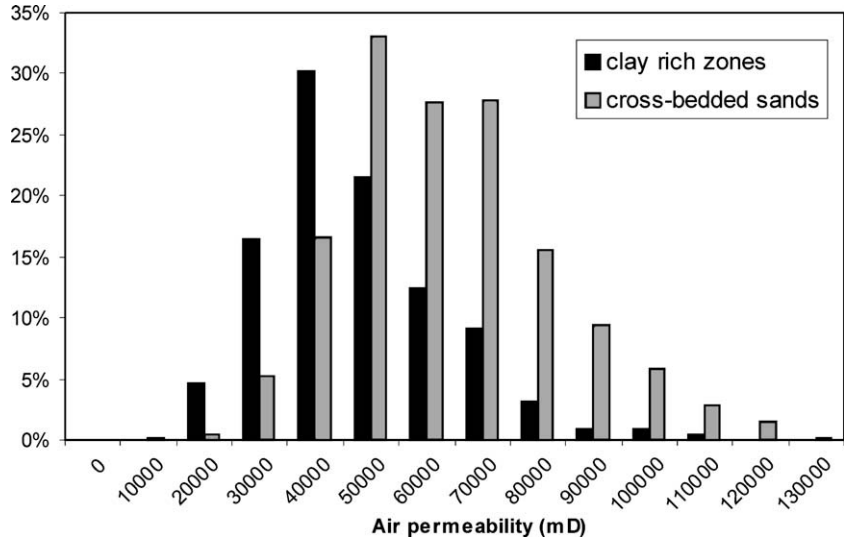

Figure 9 Combined histograms of air permeability (mD) of sand-rich and clay-rich zones.

(Bronders, 1989), which corresponds to intrinsic permeability values between 675 and 40,000 mD. Permeability values measured using the in situ air permeameter are thus characterized by a higher average value and a higher variability than the values derived from well tests. The higher average value is logical since the Bierbeek quarry is located in one of the coarsest and most permeable facies of the Brussels Sands (Houthuys, 1990). The higher variability of the air permeability measurements is related to the measurement scale. Since the well tests have a much larger measurement volume than the air permeability measurements, permeabilities measured by well tests are averages of permeabilities in this large measurement volume and show less variability than smaller scale measurements.

Relation between sedimentary structures and permeability

Relationships between measured air permeability and observed sedimentary structures were studied. First, results of individual measurements grids at different locations are discussed separately. Second, all 2750 measurements are compiled and analyzed statistically and geostatistically.

Figs. 6 and 7 show the results of observations of sedimentary structures and measurements of permeability on a 1 m by 1 m regular grid on a N40°E oriented face. On this grid, 400 air permeability measurements were made at a spacing of 5 cm. Different lithologies are present on this grid: cross-bedded sands, clay-rich bottomsets, distinct mud drapes and cemented concretions. At some locations, measuring permeability was impossible due to irregular shaped concretions, surface conditions or vegetation. Fig. 7 shows measured air permeability and interpreted lithology. A clear relationship between air permeability and lithology is observed. High permeability values, i.e. more than 70,000 mD, are measured in the cross-bedded sands. The lowest permeability values, i.e. lower than 20,000 mD are measured in the clay-rich zones, i.e. the bottomsets and distinct mud drapes. The visual distinction between sand-rich and clay-rich zones that was made in situ based on sediment characteristics is thus relevant for determining different permeability classes. The permeability values of the clay-rich zones are higher than pure clay permeability because these zones do not consist of pure clay. From grain size measurements from the work of Houthuys (1990), we know that in the ''clay-rich'' zones the silt and clay fraction is approximately 20%.

Fig. 8 shows air permeability measurements at a different location made at a smaller spacing. On a 0.6 m by 0.6 m regular grid on a N40°E oriented face, 900 air permeability measurements were made at a spacing of 2 cm. Fig. 8a shows the permeability measurements of this grid plotted on a picture of the quarry wall and Fig. 8b shows the sample variogram map of measured air permeability which helps quantify spatial correlation for different orientations by contouring variogram values computed in different directions. Lamination dip is measured at nine random locations in this grid and ranges from 19° to 33° with an

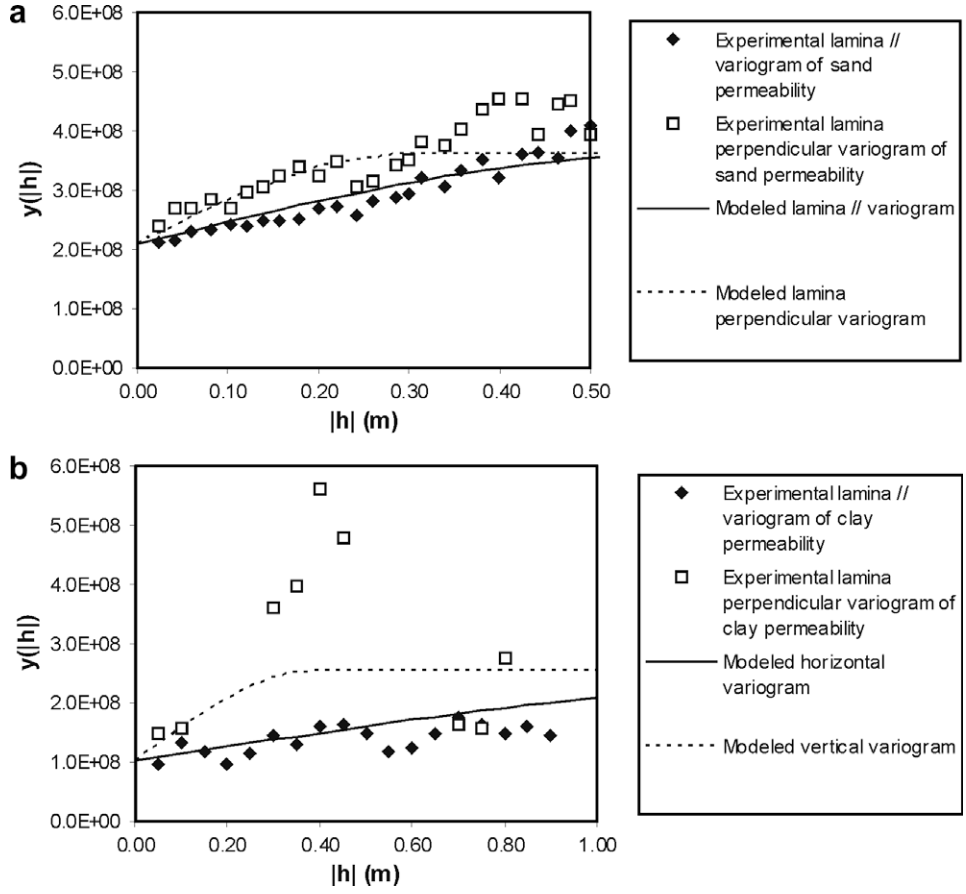

Figure 10 Combined variograms of air permeability (mD) of (a) sand-rich and (b) clay-rich zones.

average value of 26°. These figures show an obvious relationship between permeability anisotropy and lamination dip. The orientation of strongest spatial correlation in the experimental variogram corresponds exactly to the dip direction of the foreset laminae. This shows that local anisotropy within the cross-bedded sands is determined by foreset lamination.

All 2750 measurements were compiled to obtain histograms and variograms of permeability in the previously defined sand-rich and clay-rich zones (Table 1). Sand and clay permeability both display a slightly skewed distribution and differ from each other regarding their mean value and spread. Sand permeability displays a higher average permeability and a higher variance. The sand permeability distribution has an average of 58,700 mD and a variance of 3.6e8 mD^2. The permeability distribution of the clay-rich zones has an average of 42,200 mD and a variance of 2.5e8 mD^2 (Fig. 9). Permeability variograms for the sand-rich and the clay-rich zones parallel and perpendicular to bedding are shown in Fig. 10. The variograms parallel to bedding are based on data couples with different orientations parallel to bedding since permeability shows no anisotropy in planes parallel to bedding. Sand permeability displays a different spatial structure than permeability of the clay-rich zones. The experimental sand variogram shows a clear spatial structure and is modeled as a spherical model with a nugget of 2.09e8 and a sill of 1.51e8. The range parallel to bedding is 0.6 m; the range perpendicular to bedding is 0.3 m. The experimental clay variogram shows a clear spatial structure parallel to bedding but is more noisy in the perpendicular to bedding due to the limited number of available data pairs in this direction. The experimental variogram of the clay-rich zone is modeled as a spherical model with a nugget of 1.03e8 and a sill of 1.52e8. The range parallel to bedding is 1.9 m; the range perpendicular to bedding is 0.4 m (Fig. 10). Permeability in the clay-rich zones thus shows higher anisotropy and larger continuity.

Conclusions

In this study, the relation between sedimentary structures and air permeability measurements obtained at a Brussels Sands quarry was investigated. The results show that small-scale sedimentary heterogeneity induces permeability heterogeneity and anisotropy. The geometry of the sedimentary structures has a dominant control on the spatial distribution of air permeability. The visually identified clay-rich features such as bottomsets and thick mud drapes exhibit a lower permeability and a more continuous spatial permeability distribution compared to the other lithofacies in the cross-bedded sands. This means that these clay-rich layers can act as flow barriers and compartmentalize the aquifer. Moreover, variogram map analysis of the air permeability data shows that permeability anisotropy in the cross-bedded lithofacies is dominated by the foreset lamination orientation.

Although geologists in the past have known that such a relationship between sedimentary features and permeability exists in deposits like the Brussels Sands, this quantifies the relation by analyzing 2750 permeability measurements within the sedimentological context. These results provide a good basis for further research. Now that the permeability heterogeneity due to small-scale sedimentary structures is quantified, the effect of this permeability on groundwater flow and solute transport in the Brussels sands can be investigated and modeled. In a second part of this research project, the effect on the small-scale heterogeneity on larger scale permeability anisotropy and on groundwater flow and transport at different scales will be investigated. These results are also significant to the many other aquifers in the world displaying complex small-scale sedimentary structures.

Acknowledgements

The authors wish to acknowledge the Fund for Scientific Research — Flanders for providing a Postdoctoral Fellowship to the first author.

References

Anderson, M., 1989. Hydrogeological facies models to delineate large-scale spatial trends in glacial and glaciofluvial sediments. Geol. Soc. Am. Bull. 101, 501—511.

Bronders, J., 1989. Bijdrage tot de geohydrologie van Midden België door middel van geostatistische analyse en een numeriek model. PhD thesis, Vrije Universiteit Brussel, Brussel.

Castle, J.W., Molz, F.J., Lu, S., Dinwiddie, C.L., 2004. Sedimentological and fractal-based analysis of permeability data, John Henry Member, Straight Cliffs Formation (Upper Cretaceous), Utah, USA. J. Sed. Res. 74 (2), 270—284.

Davis, J.M., Lohmann, R.C., Phillips, F.M., Wilson, J.L., Love, D.W., 1993. Architecture of the Sierra Ladrones Formation, central New Mexico: depositional controls on the permeability correlation structure. Geol. Soc. Am. Bull. 105, 998—1007.

Davis, J.M., Wilson, J.L., Phillips, F.M., Gotkowitz, M.B., 1997. Relationship between fluvial bounding surfaces and the permeability correlation structure. Water Resour. Res. 33 (8), 1846—1854.

Deutsch, C.V., Journel, A.G., 1998. GSLIB Geostatistical Software Library and User's Guide. Oxford University Press, New York.

Dreyer, T., Scheie, A., Walderhaug, O., 1990. Minipermeameter-based study of permeability trends in channel sand bodies. AAPG Bull. 74, 359—374.

Dykstra, H., Parsons, R.L., 1950. The prediction of oil recovery by waterflood. In: Secondary Recovery of Oil in the United States, second ed. Am. Petrol. Inst., Washington, p. 160.

Eijpe, R., Weber, K.J., 1971. Mini-permeameters for consolidated rock and unconsolidated sand. AAPG Bull. 55, 307—309.

Fogg, G.E., Noyes, C.D., Carle, S.F., 1998. Geologically based model of heterogeneous hydraulic conductivity in an alluvial setting. Hydrogeol. J. 6 (1), 131—143.

Goggin, D.J., Chandles, M.A., Kocurek, G., Lake, L.W., 1988a. Patterns of permeability in eolian deposits: Page Sandstone (Jurassic), NE Arizone. SPE Formation Eval. 3, 297—306.

Goggin, D.J., Thrasher, R.L., Lake, L.W., 1988b. A theoretical and experimental analysis of minipermeameter response including gas slippage and high velocity flow effects. In Situ 12, 79—116.

Halvorsen, C., Hurst, A., 1990. Principles, practice and applications of laboratory minipermeametry. In: Worthington, P.F. (Ed.), Advances in Core Evaluation Accuracy and Precision in Reserves Estimation. Gordon & Breach, Amsterdam, pp. 521—549.

Hartkamp, C.A., Arribas, J., Tortosa, A., 1993. Grain-size, composition, porosity and permeability contrasts within cross-bedded

sandstones in tertiary fluvial deposits, Central Spain. Sedimentology 40 (4), 787—799.

Heinz, J., Kleineidam, S., Teutsch, G., Aigner, T., 2003. Heterogeneity patterns of Quaternary glaciofluvial gravel bodies (SW-Germany): application to hydrogeology. Sediment. Geol. 158, 1—23.

Houthuys, R., 1990. Vergelijkende studie van de afzettingsstruktuur van getijdenzanden uit het Eoceen en van de huidige Vlaamse banken. Aardkundige Mededelingen 5. Leuven University Press, p. 137.

Hurst, A., Goggin, D.J., 1995. Probe permeametry: an overview and bibliography. Am. Assoc. Petrol. Geol. Bull. 79, 463—473.

Jacobsen, T., Rendall, H., 1991. Permeability patterns in some fluvial sandstones. An outcrop study from Yorkshire, northeast England. In: Lake, L.W., Carroll, H.B. Jr., Wesson, T.C. (Eds.), Reservoir Characterization II. Academic Press, San Diego, pp. 315—338.

Jensen, J.L., Corbett, P.W.M., Pickup, G.E., Ringrose, P.S., 1996. Permeability semivariograms, geological structure and flow performance. Math. Geol. 28 (4), 419—435.

Jensen, J.L., Glasbey, C.A., Corbett, P.W.M., 1994. On the interaction of geology, measurement, and statistical-analysis of small-scale permeability measurements. Terra Nova 6 (4), 397—403.

Koltermann, C.E., Gorelick, S., 1996. Heterogeneity in sedimentary deposits: a review of structure imitating, process-imitation, and descriptive approaches. Water Resour. Res. 32 (9), 2617—2658.

Klingbeil, R., Kleineidam, S., Asprion, U., Aigner, T., Teutsch, G., 1999. Relating lithofacies to hydrofacies: outcrop-based hydrogeological characterisation of quaternary gravel deposits. Sediment. Geol. 129 (3-4), 299—310.

McKinley, J.M., Lloyd, C.D., Ruffell, A.H., 2004. Use of variography in permeability characterisation of visually homogeneous sandstone reservoirs with examples from outcrop studies. Math. Geol. 36 (7), 761—779.

Mikes, D., 2006. Sampling procedure for small-scale heterogeneities (cross-bedding) for reservoir modeling. Mar. Petrol. Geol. 23 (9—10), 961—977.

Morton, K., Thomas, S., Corbett, P., Davies, D., 2002. Detailed analysis of probe permeameter and vertical interference test permeability measurements in a heterogeneous reservoir. Petrol. Geosci. 8, 209—216.

Pannatier, Y., 1996. Variowin — Software for Spatial Data Analysis in 2D. Springer, New York, p. 91.

Remy, N., 2004. Geostatistical Earth Modeling Software: User's Manual. Stanford University, p. 87.

Ritzi, R.W., Dai, Z., Dominic, D.F., Rubin, Y.N., 2003. Review of permeability in buried-valley aquifers: centimeter to kilometer scales. In: Kovar, K., Hrkal, Z. (Eds.), Calibration and Reliability in Groundwater Modelling: A Few Steps Closer to Reality, IAHS Publication Number 277. IAHS Press, Wallingford, UK, pp. 409—418.

Ritzi, R.W., Dai, Z., Dominic, D.F., 2004. Spatial correlation of permeability in cross-stratified sediment with hierarchical architecture. Water Resour. Res. 40 (3), W03513. doi:10.1029/20WR00242.

Sturgeon, G.M., Davis, J.M., Linder, E., Harter, R.D., 2006. Heterogeneities in glaciofluvial deposits using an example from New Hampshire. Ground Water 44 (4), 528—539.

Tidwell, V.C., Wilson, J.L., 1999. Upscaling experiments conducted on a block of volcanic tuff: results for a bimodal permeability distribution. Water Resour. Res. 35 (11), 3375—3387.

Tipping, R.G., Runkel, A.C., Alexander, J.E.C., Alexander, S.C., Green, J.A., 2006. Evidence for hydraulic heterogeneity and anisotropy in the mostly carbonate Prairie du Chien Group, southeastern Minnesota, USA. Sediment. Geol. 184 (3—4), 305—330.

Van den Berg, E.H., de Vries, J.J., 2003. Influence of grain fabric and lamination on the anisotropy of hydraulic conductivity in unconsolidated dune sands. J. Hydrol. 283, 244—266.

Whittow, J.B., 2000. The Penguin Dictionary of Physical Geography. Penguin Books Ltd.

Willis, B.J., White, C.D., 2000. Quantitative outcrop data for flow simulation. J. Sediment. Res. 70, 788—802.

Zheng, C.M., Gorelick, S.M., 2003. Analysis of solute transport in flow fields influenced by preferential flowpaths at the decimeter scale. Ground Water 41 (2), 142—155.

Zinn, B., Harvey, C.F., Meigs, L., Haggerty, R., Peplinski, W., von Schwerin, C.F., 2004. Experimental visualization of solute transport and mass transfer processes in spatially heterogeneous porous media. Environ. Sci. Technol. 38 (14), 3916—3926.